RSC Advances

ROYAL SOCIETY OF CHEMISTRY

www.rsc.org/advances

Journal of Materials Chemistry A

RSCPublishing

ARTICLE

Facile synthesis of PVP-assisted PtRu/RGO nanocomposites with high electrocatalytic performance for methanol oxidation†

Cite this: DOI: 10.1039/x0xx00000x

Received ooth January 2012,
Accepted ooth January 2012

DOI: 10.1039/x0xx00000x

www.rsc.org/

Duan Bin,[a] Fangfang Ren,[a] Huiwen Wang,[a] Ke Zhang,[a] Beibei Yang,[a] Chunyang Zhai,[a] Mingshan Zhu,[b*] Ping Yang[a] and Yukou Du [a*]

In this paper, we report a facile approach for the synthesis of polyvinylpyrrolidone (PVP)-stabilized PtRu/RGO nanocomposites (PtRu/RGO/PVP) by one-pot method. The structure, morphology and composition of as-prepared catalysts were characterized by Raman, transmission electron microscopy (TEM) and energy dispersive X-ray spectroscopy (EDX), respectively. It is found that PVP plays an important role in controlling the size of PtRu nanoparticles (NPs) as well as their dispersion stability. TEM images show that as-prepared PtRu NPs with mean particle size of about 3.09 nm are uniformly dispersed on RGO surface in the presence of PVP. The electrocatalytic properties of the as-prepared catalysts were evaluated by cyclic voltammetry (CV) and chronoamperometry (CA). Compared to PtRu/RGO and PtRu/PVP catalysts, our PtRu/RGO/PVP hybrids exhibit evidently enhanced electrocatalytic activity and stability for the methanol oxidation reaction. Moreover, our multicomposites also show higher electrocatalytic performance than the commercial PtRu/C catalysts. The PtRu/RGO/PVP nanostructures with an optimized molar ratio of Pt/Ru (1:1) display 1.96 times than the commercial PtRu/C nanospecies. These findings indicate that the PtRu/RGO catalysts show a promising future of potential applications in direct methanol fuel cells with assistance of PVP stabilized.

1. Introduction

Due to the continuous consumption of fossil fuel and the increasing environment pollution caused by the traditional fuel utilization, direct methanol fuel cells (DMFCs) have recently aroused considerable attention and interest as portable devices with characteristics of high energy density at low operation temperature and pollutant emission.[1-6] At present, pure Pt is qualified to the be most active anodic catalyst due to its excellent performance during methanol oxidation.[2-5] Unfortunately, the high price of pure Pt and the catalyst poisoning by the CO-like intermediates during the oxidation of methanol hinder the widely commercialization of DMFCs.[2-5]

Great efforts have been made to decrease the usage of noble metal Pt nanoparticles (NPs) and increase its electrocatalytic performance towards methanol oxidation.[2-6] One widely accepted strategy is to fabricate Pt-based binary catalyst by employing a second metal such as metallic Ru. Many studies have demonstrated that the catalytic activity and stability of Pt-Ru catalyst could be evidently enhanced, which could be ascribed to the bifunctional mechanism or electronic effect. [4,5,7-16] Another strategy is to adopt catalyst supports to increase the electrochemical active surface area (ECSA) and good dispersion for supporting the metal NPs. Various carbon nanomaterials such as carbon black, carbon nanotube (CNT), graphene and their derivatives have been served as catalyst supports both academically and commercially.[6] Among these supports, graphene has recently received increasing attention and has been certified to be a promising candidate as a catalyst support due to its extremely high specific surface area, excellent electrical conductivity and superior chemical stability.[19,20] These outstanding performances propel us to consider graphene as an ideal substitute for other carbon materials in fuel cells.

To date, several graphene hybridized Pt-Ru nanocomposites have been developed for improving electrocatalytic performance.[19,20] For example, Dong et al. have firstly reported PtRu nanoparticles with 10 nm supported on graphene with high electrocatalytic performances for methanol and ethanol oxidation.[8] Kim and co-authors have reported efficient electrooxidation of glycerol over a PtRu/graphene catalyst.[11] Zhao et al. have synthesized highly dispersed PtRu/graphene catalysts, which prepared via supercritical carbon dioxide–methanol route.[13] Liu group have reported that uniformly distributed PtRu NPs were decorated on the N-doped

graphene aerogel with porous structures.[16] Nevertheless, it should be point out that the synthetic condition, size and dispersion of metal NPs and catalytic stability for methanol oxidation is still not very satisfactory for further application.

Currently, surfactant as a stabilizer for preventing the metal colloids from aggregation and improving the deposition of the colloids onto the carbon support received more and more attentions.[17,18] For example, Hwang group reported that graphite carbon nanofibers hybridized with PtRu NPs as promising catalysts with assistance of polyvinylpyrrolidone (PVP) surfactant.[18] The PVP stabilized nanocomposites could efficiently enhance the electrocatalytic performance towards methanol oxidation. More recently, surfactant-assistant graphene-based catalysts could distinctly enhance catalytic activity and stability since that surfactant could efficiently improve the solubility and aggregation prevention of graphene.[21] Herein, we develop a one-pot method prepares well-dispersion PtRu NPs with 3.09 nm size supported on the graphene surface in the presence of PVP surfactant. Compared with the bare PtRu/RGO nanospecies, our PVP assisted PtRu/RGO NPs not only show well-separated with small size of 3.09 nm but also show nice-stability (even stable for more than one year and well re-dispersion). Moreover, this multicomposite displays distinctly improved electrocatalytic activity and stability for PtRu/RGO, PtRu/PVP and commercial PtRu/C nanostructures. With an optimized molar ratio of Pt/Ru (1:1), the PtRu/RGO/PVP nanostructures show 1.96 times than the commercial PtRu/C nanospecies. Our investigation might initiate new opportunities for constructing graphene-based materials with enhanced electrocatalytic performance and stability under surfactant assistance and show a promising future of potential applications in direct methanol fuel cells.

2. Experimental

2.1 Chemicals

Graphite powder (Sinopharm Chemicals Reagent Co., Ltd, China) was used as received. Commercial PtRu/C catalysts (JM 30% PtRu, Hispcc5000, Shanghai Hesen Electric Co., Ltd., China), $H_2PtCl_6 \cdot 6H_2O$ and $RuCl_3$ (Shanghai Shiyi Chemicals Reagent Co., Ltd., China), $NaNO_3$, $KMnO_4$, H_2O_2 (30%), CH_3OH, H_2SO_4 (95%), polyvinylpyrrolidone (PVP, K30), $NaBH_4$ and other reagents were all of analytical grade purity. All aqueous solutions were prepared with double distilled water.

2.2 Preparation of graphene oxide (GO)

GO was prepared from natural graphite powder by a modified Hummers method.[22] Firstly, 1.0 g graphite powder and 0.5 g $NaNO_3$ were added into 24 mL concentrated H_2SO_4 solution with stirring in an ice bath. Then, 3.0 g $KMnO_4$ was slowly added into the solution and the mixture was stirred at 20 °C for 30 min. After that, the temperature of the solution was increased to 35 °C under vigorous stirring for another 30 min, followed by the slow addition of 46 mL of secondary distilled water. Then the temperature was raised to 98 °C and further stirred for 15 min. The reaction was then terminated by adding 140 mL doubly distilled water after 10 mL 30% H_2O_2 solution was added. Finally, the resulting solution was filtered and washed with 5% HCl until sulfate ions could not be detected with $BaCl_2$. The sample was dried in a vacuum at 40 °C for 12 hours to obtain the final product of GO.

2.3 Synthesis of PVP stabilized PtRu/reduced graphene oxide (PtRu/RGO/PVP) nanocomposites

The PVP stabilized PtRu/RGO nanocomposites were synthesized by using one-pot method, where $NaBH_4$ was as the reducing agent. The preparation process is described as follows, 5 mL of 4.0 mg mL^{-1} GO and 0.01 g of PVP were dissolved in 20 mL of water accompanied by vigorous stirring for 30 minutes. Then an aqueous solution of 4 mL H_2PtCl_6 (7.723×10^{-3} mol L^{-1}) and 1.6 mL $RuCl_3$ (19.2×10^{-3} mol L^{-1}) with the molar of ratio of Pt to Ru was 1:1 was added to the above mixture under stirring for 1 h. Subsequently, 5 mL of freshly prepared $NaBH_4$ (6 mg mL^{-1}) aqueous solution was added dropwise under vigorous stirring for another 4 h at an ambient temperature. The resulting black turbid liquid was centrifuged and repeatedly washed with deionized water and ethanol to remove excess $NaBH_4$, which was then dried for 8 h in a vacuum at 25 °C to obtain the solid product. Finally, the as-prepared catalyst powders were dispersed in 10 mL deionized water and treated ultrasonically for 30 min to obtain the catalyst ink. The obtained catalyst was denoted as PtRu (1:1)/RGO/PVP. For comparison, the PtRu (1:1)/PVP, PtRu (1:1)/RGO, PtRu (1:2)/RGO/PVP, PtRu (2:1)/RGO/PVP and Pt/RGO/PVP were also prepared by the same procedure. All the catalysts contain a total metal (Pt, Pt+Ru) loading of 31%.

2.4 Materials characterization

Digital pictures of reaction process were taken with digital camera. The Raman spectra of these samples were recorded at room temperature on a RM2000 microscopic confocal Raman spectrometer with argon-ion laser at the excitation wavelength of 633 nm. The X–ray diffraction (XRD) measurements were performed on a PANalytical X' Pert PRO MRD system with Cu Ka radiation (k =1.54056 Å) operated at 40 kV and 30 mA. The morphologies of these samples were characterized using a TECNAI-G20 electron microscope (TEM) with an accelerating voltage of 200 kV. High-resolution TEM (HRTEM) images were obtained with a JEM-2100F high-resolution transmission electron microscope operating at 200 kV. TEM samples were prepared by placing a drop of the colloid dispersion onto a copper grid covered with a perforated carbon film and then evaporating the solvent. The energy dispersive X-ray (EDX) analysis was conducted with a Horiba EMAX X-act energy dispersive spectroscope that was attached to the S-4700 system. All of the measurements were carried out at room temperature.

2.5 Electrochemical measurements

All electrochemical measurements were carried out with a CHI 660B electrochemical workstation. A conventional three-electrode system was used with platinum wire, saturated calomel electrode (SCE) and a glassy carbon electrode (GCE, 3 mm diameter) as the counter, reference and working electrodes, respectively. The working electrode was prepared by dropping

20 μL of the composites catalyst ink onto the surface of GCE and dried at room temperature. In this paper, the amount of total metal in glassy carbon was controlled as 0.25 mg cm^{-2}. For the electrochemical active surface area (ECSA) study, cyclic voltammetry (CV) measurements of the catalysts were conducted in a solution of 0.5 M H_2SO_4 solution at a scan of 50 mV s^{-1} for 20 cycles from -0.25 V to 1.0 V. The ECSA value can be calculated by integrating the hydrogen adsorption/desorption area between -0.25 V to 0.1 V. The specific ECSA was derived from the following equation:[23]

$$ECSA = \frac{Q_H}{0.21 \times m}$$

Q_H represents the average charge for hydrogen adsorption and desorption, which was theoretically evaluated under the CV curve by $Q_H = \int IdE / v$ (v is the scanning rate), m is the loading amount of metal, 0.21 mC cm^{-2} is Pt crystalline activity surface area transferred coefficient. The electrochemical activity of methanol oxidation reaction was measured by linear sweep voltammetry at a scan of 50 mV^{-1} for 20 runs from -0.2 V to 1.0 V. Chronoamperometry (CA) measurements were conducted at 0.6 V for 1500 s. All solutions were deaerated by a dry nitrogen stream and maintained with a slight overpressure of nitrogen during the whole experiment.

3. Results and discussion

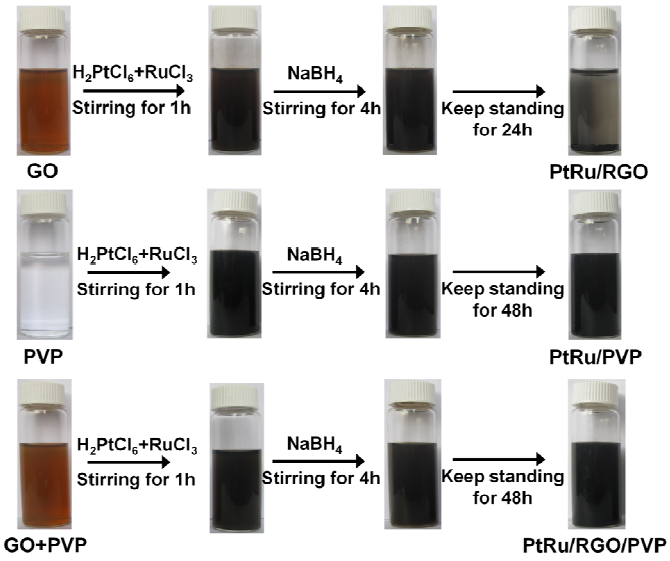

Fig. 1 Digital photos of the synthetic process of the PtRu/RGO, PtRu/PVP and PtRu/RGO/PVP NPs.

Experimentally, the PVP stabilized PtRu/RGO composites were synthesized by using one-pot method, where $NaBH_4$ was worked as reduced agent. Firstly, when GO as stabilizer, in the presence of $NaBH_4$, the noble metal NPs could efficient reduced from the H_2PtCl_6 and $RuCl_3$ precursor, as shown in Fig. 1. At the same time, the GO nanosheets are also reduced to reduced graphene oxide (RGO) when $NaBH_4$ solution was dropped into the mix solution.[24] However, it easy can be seen that the generated noble metal NPs are obvious aggregated and gradually settled after 24 h. In the presence of PVP (Fig. 1b and 1c), the generated noble metal NPs disperse well in the aqueous solution even stay for several months. Generally, PVP was used as typical stabilizer for the preparation of noble metal nanoclusters. Accordingly, the PVP could efficient protect the noble metal NPs from aggregation and improve aqueous dispersion.

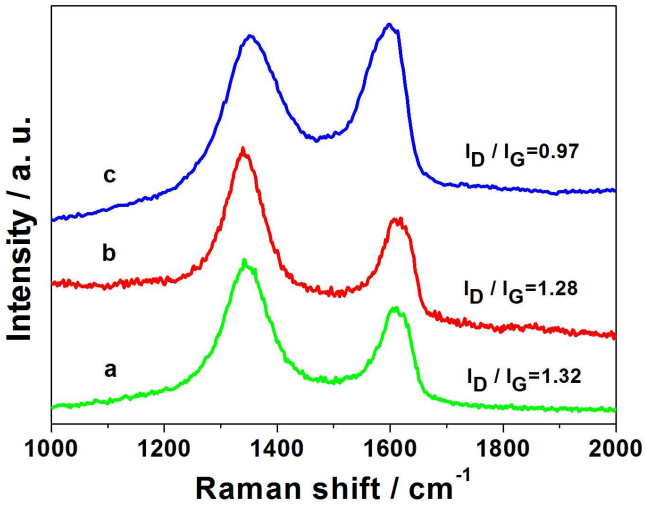

Fig. 2 Raman spectra of GO sheets (a), PtRu/RGO (b) and PtRu/RGO/PVP (c) nanostructures.

Raman spectrum is a powerful tool to characterize the structure of graphene materials, and the corresponding results of GO sheets and our graphene-based materials are displayed in Fig. 2. All three samples exhibit two prominent peaks at approximately 1350 cm^{-1} and 1598 cm^{-1}, which are attributed to the D and G bands of graphene sheets, respectively.[25,26] The D band is usually related to the breathing mode of k-point phonons of A_{1g} symmetry, while the G band is associated with the E_{2g} vibration mode of sp^2 carbon domains.[25,26] The G band was broadened and shifted towards a slightly higher wave number from GO to RGO, which was probably caused by stress in solution.[27] When the GO is chemically reduced, the conjugated graphene network (sp^2 carbon) will be reestablished, the intensity ratio of the D and G bands (D/G) increases further because the size of reestablished graphene network becomes smaller than the original.[25,26] The peak intensity ratios (I_D/I_G) are estimated to be 1.32, 1.28, and 0.97 for the PtRu /RGO/PVP, PtRu/RGO and bare GO samples, respectively. Clearly, the PtRu/RGO/PVP and PtRu/RGO catalysts show a higher I_D/I_G value than that of GO, which demonstrates the effective reduction of GO. Additionally, the I_D/I_G value of PtRu/RGO/PVP hybrids did not change obviously at the existence of PVP, indicating that the graphene nanosheet did not reduce the size in-plane sp^2 domains greatly.[28]

The morphology and structural features of the PtRu/RGO/PVP, PtRu/RGO and PtRu/PVP catalysts were characterized by TEM analysis. It can be seen from Fig. 3a and 3b that PtRu NPs are homogeneously distributed on the surface of RGO sheets without obvious agglomeration, suggesting the perfect combination between

metal NPs and RGO sheets. The corresponding histogram of particles size distribution in Fig. S1 shows that the PtRu NPs supported on RGO/PVP have a mean diameter of about 3.09 nm. Additionally, the metal NPs in PtRu/PVP composites also present a narrow particles size of about 3.21 nm in Fig. 3c. However, as observed from the TEM image shown in Fig. 3d, PtRu NPs underwent severe aggregation in the PtRu/RGO composites and kept some irregular particles with the average particle size of 5.84 nm, which is much bigger than that of PtRu/RGO/PVP composites. These results illustrate that the addition of PVP is help to prevent PtRu NPs from aggregating and restacking, thereby leading to smaller particle size.[29]

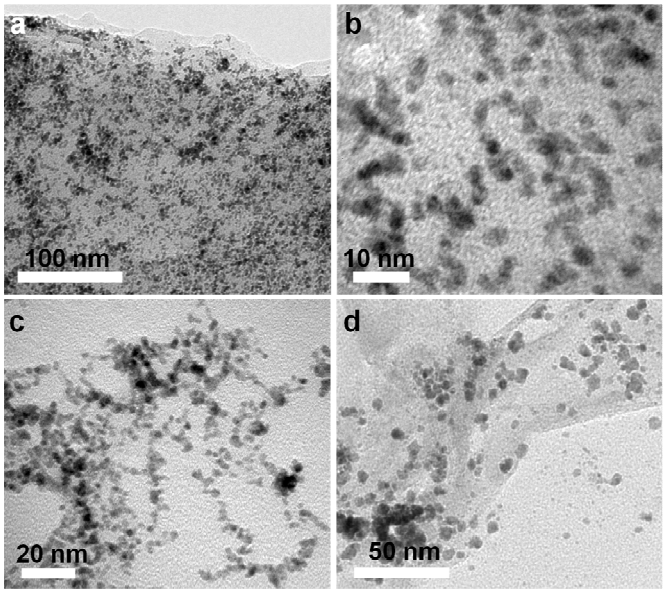

Fig. 3 TEM images PtRu/RGO/PVP (a and b), PtRu/PVP (c) and PtRu/RGO (d) nanostructures.

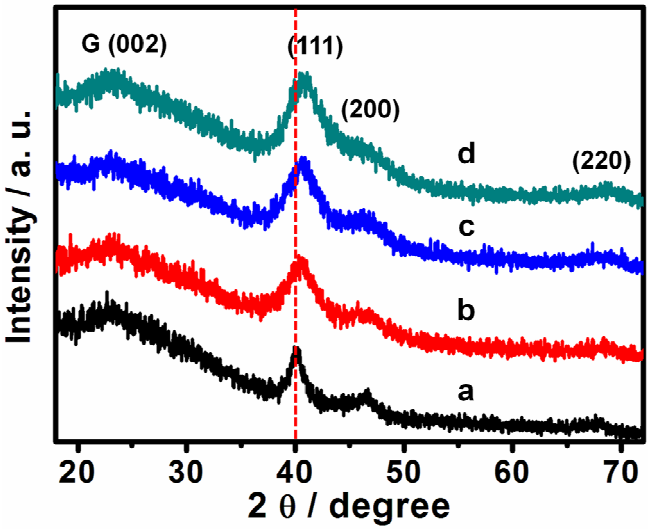

Fig. 4 XRD patterns of Pt/RGO/PVP (a), PtRu (2:1)/RGO/PVP (b), PtRu (1:1)/RGO/PVP (c) and PtRu (1:2)/RGO/PVP (d) NPs.

To prove the generation of PtRu alloy, XRD patterns of Pt/RGO/PVP and various ratios of PtRu/RGO/PVP NPs were investigated. As shown in Fig. 4, for bare Pt/RGO/PVP, the peaks of 39.9°, 46.8° and 67.9° are corresponded to the diffraction of the (111), (200) and (220) crystal planes of Pt (JCPDS NO. 04–0802), respectively.[30] When the Ru atoms were introduced, it can be seen that the diffraction peaks slightly shift to higher degree in the order of Pt/RGO/PVP, PtRu (2:1)/RGO/PVP, PtRu (1:1)/RGO/PVP and PtRu (1:2)/RGO/PVP (Fig. S2), which indicates the decrease of the lattice constant with the increase of Ru concentration. The position of Pt (111) shifts from 39.9° to 40.8°, which indicates the formation of a bimetallic PtRu alloy in our experiment (Fig. S2).[12,17] Moreover, beside the diffraction peaks of Pt or PtRu alloy, the peak at *ca.* 23.2° is the characteristic peak of RGO nanosheets,[31] which suggests the presence of graphene in our samples.

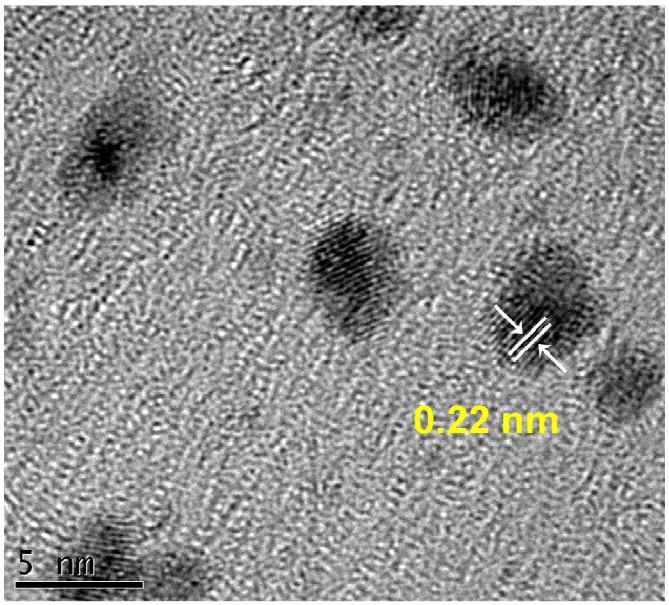

Fig. 5 High-resolution TEM image of PtRu/RGO/PVP NPs.

The HRTEM image further reveals that PtRu alloys are crystalline with lattice structures. Generally, the lattice fingers with d-spacing of 0.226 nm can be attributed to (111) plane of fcc Pt.[32]As shown in Fig. 5, the lattice distance for our PtRu/RGO/PVP NPs is measured to be 0.22 nm, which is slightly smaller than that of monometallic Pt. Furthermore, the lattice fringes with a lattice spacing of ca. 0.22 nm match with the above (111) plane of PtRu/RGO/PVP. This result further indicates the formation of PtRu alloy in our synthetic process. The chemical composition of the PtRu/RGO/PVP composites was analyzed by EDX spectrum, and the results shown in Fig. S3. The existence of C and O are ascribed to the base plane and oxygenated groups of the RGO, respectively. The spectrum reveals that the atom ratio Pt to Ru is about 1.075, which is very closed to the theoretical value (1:1), further suggesting the generated PtRu alloy.

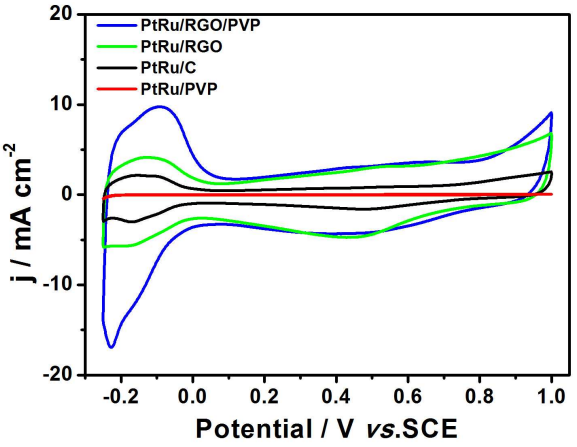

Fig. 6 CVs of PtRu/RGO/PVP, PtRu/RGO, PtRu/PVP, PtRu/C catalysts in 0.5 M H_2SO_4 solution at a scan of 50 mV s^{-1}.

The electrochemical performances of the PtRu/RGO/PVP, PtRu/RGO and PtRu/PVP catalysts were evaluated by CV analysis in 0.5 M H_2SO_4 solution. As plotted in Fig. 6 and summarized in Table 1, by integrating the charge in the adsorption/desorption region of hydrogen, we can estimate the value of ECSA is 55.38 m^2 g^{-1} for PtRu/RGO/PVP. Interesting, it was found that the PtRu/PVP catalysts show negligible ECSA value (3.55 m^2 g^{-1}), although the size was similar as PtRu/RGO/PVP. When PtRu/RGO nanospecies were used as electrocatalysts, the value of ECSA is estimated to be ca. 18.70 m^2 g^{-1}. This is since that the graphene sheets significantly enhance the availability ECSA of electrocatalyst for electron transfer.[33] The larger ECSA of PtRu/RGO/PVP means that it has more active sites compared other composites. These results suggested that in the PtRu/RGO/PVP system, the PVP could decrease the size of metal NPs, which increase the density of active sites on the electrode surface, and RGO could improve charger transfer efficiently. The PVP and RGO synergically contributed to the enhanced electrocatalytic performance. Moreover, our PtRu/RGO/PVP electrode displays 5 times ECSA value compared with commercial PtRu/C species (11.07 m^2 g^{-1}), suggesting that as-prepared electrode might have potential practical fuel cells application.

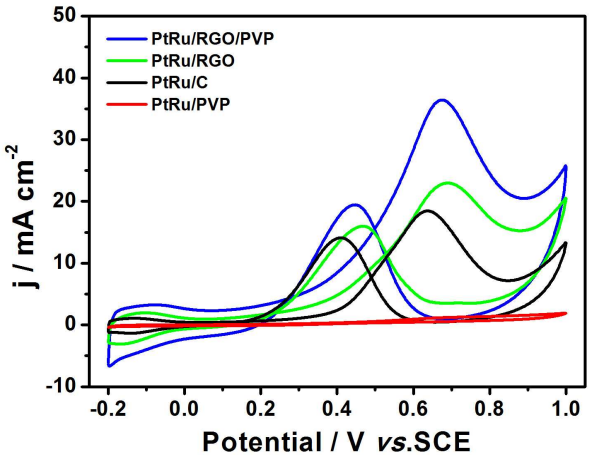

Fig. 7 CVs of PtRu/RGO/PVP, PtRu/RGO, PtRu/PVP, PtRu/C catalysts in 0.5 M H_2SO_4 +1.0 M CH_3OH solution at a scan of 50 mV s^{-1}.

Table 1 Comparison of eletrocatalytic activity of methanol oxidation on PtRu/RGO/PVP, PtRu/RGO, PtRu/PVP and commercial PtRu/C electrodes

Electrode	ECSA / m^2 g^{-1}	Forward sweep		Reverse sweep		
		I_F (mA cm^{-2})	(mA mg^{-1})$_{metal}$	I_b (mA cm^{-2})	(mA mg^{-1})$_{metal}$	I_F/I_b
PtRu/RGO/PVP	55.38	36.5	146.0	19.5	78.0	1.87
PtRu/RGO	18.70	23.1	92.4	13.0	52.0	1.78
PtRu/PVP	3.55	0.2	0.8	0.18	0.72	1.11
PtRu/C	11.07	18.6	74.4	14.2	56.8	1.31

Fig. 7 shows the CVs of methanol oxidation on the PtRu/RGO/PVP, PtRu/RGO, PtRu/PVP and commercial PtRu/C electrodes in 0.5 M H_2SO_4 containing 1.0 M CH_3OH solution. As in Fig. 7 and Table 1, the forward peak current density of methanol oxidation on PtRu/RGO/PVP (36.5 mA cm^{-2} or 146 mA mg^{-1}) is about 1.6, 29.2 and 1.96 times higher than that on PtRu/RGO (18.48 mA cm^{-2} or 92.4 mA mg^{-1}), PtRu/PVP (0.2 mA cm^{-2} or 0.8 mA mg^{-1}) and PtRu/C (18.6 mA cm^{-2} or 74.4 mA mg^{-1}), respectively. Generally, the ratio of the forward anodic peak current (I_f) to the backward cathodic peak current (I_b) usually is used to evaluate the catalyst tolerance to CO and other carbonaceous species.[34] The PtRu/RGO/PVP catalyst has a higher I_f/I_b (1.87) than PtRu/RGO (1.78) and commercial PtRu/C (1.31) catalyst. Therefore, based on the above analysis, the as-prepared PtRu/RGO/PVP shows highest electrocatalytic performance and better tolerance of the intermediate than the other catalysts. This can be mainly ascribed to two factors as follows, one factor is believed to be the improved surface area of PtRu NPs on the graphene sheets support,[35] the other could be attributed to the modification of PVP, which can prevent the PtRu NPs from aggregating in chemical reactions, leading to the formation of well-dispersed and smaller-sized PtRu NPs that provided more available active catalytic sites.

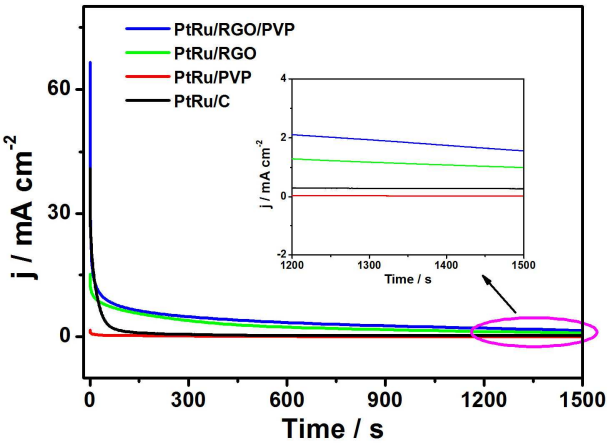

Fig. 8 Chronoamperometric curves of the PtRu/RGO/PVP, PtRu/RGO, PtRu/PVP and commercial PtRu/C catalyst at 0.6 V in 0.5 M H_2SO_4 + 1.0 M CH_3OH solution at 0.6 V for 1500 s.

Furthermore, the stabilities of the as-prepared and commercial catalysts are also studied. Fig. 8 shows the CA curves for these catalysts performed in 0.5 M H_2SO_4 + 1.0 M CH_3OH at 0.6 V for 1500 s. In initial period, the rapid current decay for all catalysts was observed because of the formation of intermediate species such as CH_3OH_{ads} and CHO_{ads} during the methanol oxidation reaction.[36] During the whole time, it is clear that the current density produced on PtRu/RGO/PVP catalyst is higher than those on PtRu/RGO, PtRu/C and PtRu/PVP catalysts. This finding indicates that the PtRu/RGO/PVP catalyst has a more durable and higher electrocatalytic activity for methanol oxidation in comparison with the other catalysts, which is also consistent with the CV results (Fig. 7).

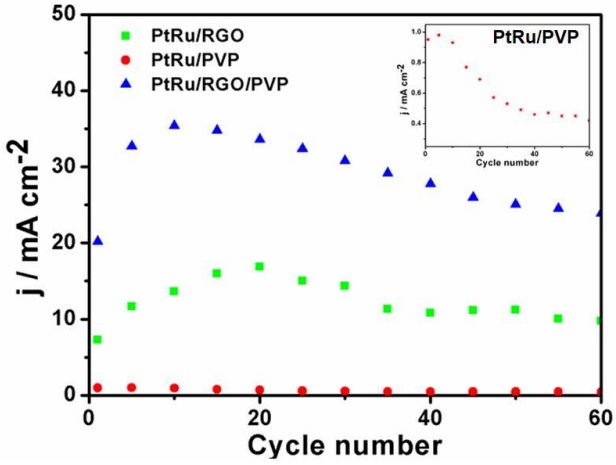

Fig. 9 Long-term electrocatalytic stabilities of PtRu/RGO/PVP, PtRu/RGO and PtRu/PVP electrodes in 0.5 M H_2SO_4 + 1.0 M CH_3OH solution at a scan of 50 mV s^{-1}. The inset of enlarge electrocatalytic stability of spectrum of PtRu/PVP electrode.

In fact, the long term of stability of a catalyst is crucial. CVs of 100 cycles for the PtRu/RGO/PVP, PtRu/RGO and PtRu/PVP electrodes were performed in 0.5 M H_2SO_4+1.0 M CH_3OH solution at a scan of 50 mVs^{-1}. The forward peak current densities as a function of cyclic scan number are shown in Fig. 10. All catalysts exhibit an increased peak current densities at the initial cycle and then slowly decrease as the continuing increase of the cycle number, which is attributed to the poison by CO-likes species and some dissolution loss of platinum.[37] For PtRu/RGO/PVP catalyst, it can be seen that the forward oxidation peak current density approaches the maximum (35.4 mA cm^{-2}) at the 10th cycle, and then decreases to 23.9 mA cm^{-2} after 60 cycles, with a total decrease of 32.5% relative to maximum. However, the forward peak current densities after 60 cycles on PtRu/RGO and PtRu/PVP are reduced by 42.2% and 55.8%, respectively. These observations clearly indicate that the PtRu/RGO/PVP catalyst has much better long term stability for methanol oxidation than PtRu/RGO and PtRu/PVP catalysts.

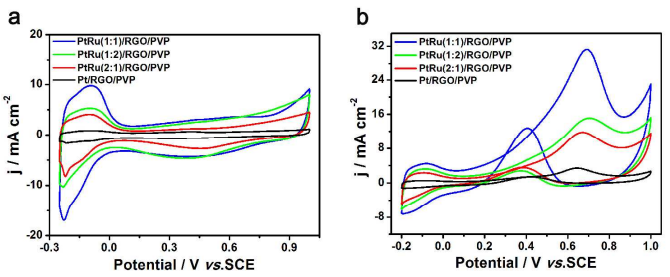

Fig. 10 (a) CVs of Pt/RGO/PVP, PtRu(1:1)/RGO/PVP, PtRu(1:2)/RGO/PVP and PtRu(2:1)/RGO/PVP catalyst in 0.5 M H_2SO_4 solution at a scan of 50 mV s^{-1}. (b) these catalysts in a mix solution of 0.5 M H_2SO_4 + 1.0 M CH_3OH at a scan of 50 mV s^{-1}.

In order to compare with the electrochemical performance of different Pt/Ru atom ratio, the CVs of various molar ratio of Pt/Ru such as Pt/RGO/PVP, PtRu (2:1)/RGO/PVP, PtRu (1:1)/RGO/PVP and PtRu (1:2)/RGO/PVP catalysts in 0.5 M H_2SO_4 solution were investigated. As shown in Fig. 8a, for all the catalysts, they appear different responses to hydrogen adsorption/desorption in the potential region between -0.25 and 0.1 V. The ECSA of PtRu (1:1)/RGO/PVP, PtRu (1:2)/RGO/PVP, PtRu (2:1)/RGO/PVP and Pt/RGO/PVP are calculated to be 55.38, 29.28, 26.04 and 4.69 m^2 g^{-1}, respectively. Obviously, the PtRu (1:1)/RGO composites exhibit the largest ECSA among these samples, which is about 11.8 times than Pt/RGO/PVP. The higher electrochemical activity surface area than pure Pt can be explained by the fact that the Pt-base catalysts contained oxophilic metal like Ru.[38] The ECSA reaches the highest value when the Pt NPs are combined by the Ru atom of at the Pt/Au molar ratio of 1:1, therefore, the PtRu (1:1)/RGO/PVP composites show better bimetallic cooperative function and increases the active sites on the electrode surface.

Fig. 10b shows the CVs for oxidation of methanol on the PtRu (1:1)/RGO/PVP, PtRu (2:1)/RGO/PVP, PtRu (1:2)/RGO/PVP and Pt/RGO/PVP modified electrodes in 0.5 M H_2SO_4 + 1 M CH_3OH solution. An anodic current peak for the oxidation of methanol was clearly detected for the forward scan of these modified electrodes. In the reverse scan, the oxidative peak current may be ascribe to the continuous oxidation of incompletely oxidized carbonaceous species intermediates accumulated on the surface of catalyst during the forward scan.[39] A weak anodic peak (3.38 mA cm^{-2}) of the Pt/RGO/PVP composites appears in the Fig. 10b, which shows lowest electrocatalytic activity for methanol oxidation. While the forward scan peak current densities of PtRu (1:1)/RGO/PVP (31.44 mA cm^{-2}), PtRu (1:2)/RGO/PVP (15.19 mA cm^{-2}) and PtRu (2:1)/RGO/PVP (11.83 mA cm^{-2}) are respectively about 9.3, 2.9 and 3.5 times higher than that of Pt/RGO/PVP. It was concluded that the capabilities of the electrocatalytic oxidation of methanol on these modified electrodes follow the order PtRu (1:1)/RGO>PtRu (1:2)/RGO>PtRu (2:1)/RGO>Pt/RGO/PVP, which is in accordance with the change trend of ECSA. From the above data, the PtRu (1:1)/RGO/PVP catalyst has the best catalytic activity among these composites.

4. Conclusions

In summary, a facile approach for synthesizing PtRu alloy catalysts by employing $NaBH_4$ as reducing agent in the presence of PVP and RGO was investigated. In the assistance of PVP and the support material-graphene, the PtRu NPs show well-separated with smaller size as well as show nice-stability and well re-dispersion. The obtained PtRu/RGO/PVP composites exhibited a remarkably enhanced catalytic performance in the methanol oxidation reaction compared with PtRu/RGO and PtRu/PVP catalysts. This is attribute to the PVP surfactant and graphene not only improve the dispersion and anti-aggregation of PtRu NPs, but also greatly enhance the electrical conductivity in the composites via the synergistic transport with PtRu NPs.The PtRu/RGO/PVP catalyst with Pt/Ru molar ratio of 1:1 exhibits the highest electrocatalytic activity. This investigation has suggested a PVP assistant PtRu/RGO system with enhanced catalytic activity and stability, which has potential applications in the fields of in DMFCs.

Acknowledgements

This work was supported by the National Natural Science Foundation of China (51373111, 51073114 and 20933007), the Opening Project of Xinjiang Key Laboratory of Electronic Information Materials and Devices (XJYS0901-2010-01), the Priority Academic Program Development of Jiangsu Higher Education Institutions (PAPD), and the Academic Award for Young Graduate Scholar of Soochow University.

Notes and References

[a] *College of Chemistry, Chemical Engineering and Materials Science, Soochow University, Suzhou 215123, P.R. China. Fax: +86 512 65880089; Tel: +86 512 65880361; E–mail: duyk@suda.edu.cn*
[b] *Institute of Chemistry, Chinese Academy of Sciences, Beijing100190, P.R. China. E–mail: zhums@iccas.ac.cn*

† Electronic Supplementary Information (ESI) available: particle-size distribution histograms and enlarge XRD pattern of our samples, EDX spectrum of PtRu/RGO/PVP. See DOI: 10.1039/b000000x/

1 A. S. Aricò, S. Srinivasan and V. Antonucci, *Fuel cells*, 2001, **1**, 133-161.
2 H. Liu, C. Song, L. Zhang, J. Zhang, H. Wang and D. P. Wilkinson, *J. Power Sources,* 2006, **155**, 95-110.
3 S. Basri, S. K. Kamarudin, W. R. W. Daud, Z. Yaakub, *Int. J. Hydrogen Energy*, 2010, **35**, 7957-7970.
4 X. Zhao, M. Yin, L. Ma, L. Liang, C. Liu, J. Liao, T. Lu and W. Xing, *Energy Environ. Sci*, 2011, 4, 2736-2753.
5 M. Cao, D. Wu and R. Cao, *ChemCatChem*, 2014, **6**, 26-45.
6 H. Huang and X. Wang, *J. Mater. Chem. A*, 2014, **2**, 6266-6291.
7 T. J. Schmidt, H. A. Gasteiger, R. J. Behm, *Electrochem. Commun*, 1999, **1**, 1-4.
8 L. Dong, R. R. S. Gari, Z. Li, M. M. Craig, S. Hou, *Carbon,* 2010, **48**, 781-787.
9 H. Li, X. Zhang, H. Pang, C. Huang, J. Chen, *J. Solid. State. Electrochem*, 2010, **14**, 2267-2274.
10 C. Nethravathi, E. A. Anumol, M. Rajamathi and N. Ravishankar, *Nanoscale*, 2013, **3**, 569-571.
11 H. J. Kim, S. M. Choi, M. H. Seo, S. Green, G. W. Huber, and W. B. Kim, *Electrochem. Commun*, 2011, **13**, 890-893.
12 H. P. Cong, X. C. Ren and S. H. Yu, *ChemCatChem*, 2012, **4**, 1555-1559.
13 J. Zhao, L. Zhang, H. Xue, Z. Wang and H. Hu, *RSC Adv*, 2012, **2**, 9651-9659.
14 H. Wang, J. Du, Z. Yao, R. Yue, C. Zhai, F. Jiang, Y. Du, C. Wang and P. Yang, *Colloids Surf., A,* 2013, **436**, 57-61.
15 S. Woo, J. Lee, S. K. Park, H. Kim, T. D. Chung and Y. Piao, *J. Power Sources*, 2013, **222**, 261-266.
16 S. Zhao, H. Yin, L. Du, G. Yin, Z. Tang and S. Liu, *J. Mater. Chem. A*, 2014, **2**, 3719-3724.
17 X. Wang and I. M. Hsing, *Electrochim. Acta*, 2002, **47**, 2981-2987.
18 Y. L. Hsin, K. C. Hwang and C. T. Yeh, *J. Am. Chem. Soc*, 2007, **129**, 9999-10010.
17 E. Antolini, *Appl. Catal. B: Eviro*, 2012, **123-124**. 52-68.
20 M. Liu, R. Zhang and W. Chen, *Chem. Rev*, 2014, **114**, 5117-5160.
21 M. Zhu, Z. Li, B. Xiao, Y. Lu, Y. Du, P. Yang and X. Wang, *ACS Appl. Mater. Interface*, 2013, **5**, 1732-1740.
22 Z. Yao, M. Zhu, F. Jiang, Y. Du, C. Wang and P. Yang, *J. Mater. Chem*, 2012, **22**, 13707-13713.
23 W. Zhou, C. Zhai, Y. Du, J. Xu and P. Yang, *Int. J. Hydrogen Energy,* 2009, **34**, 9316-9323.
24 F. Li, Y. Guo, Y. Liu, H. Qiu, X. Sun, W. Wang, Y. Liu and J. Gao, *Carbon*, 2013, **64**, 11-19.
25 C. Zhai, M. Zhu, Y. Lu, F. Ren, C. Wang, Y. Du and P. Yang, *Phys. Chem. Chem. Phys*, 2014, **16**, 14800-14807.
26 F. Ren, H. Wang, M. Zhu, W. Lu, P. Yang and Y. Du, *RSC Adv.*, 2014, **4**, 24156–24162.
27 H. L. Guo, X. F. Wang, Q. Y. Qian, F. B. Wang and X. H. Xia, *ACS Nano*, 2009, **9**, 2653-2659.
28 S. Guo, S. Dong and E. Wang, *ACS Nano*, 2010, **4**, 547-555.
29 Y. Zhang, H. Shu, G. Chang, K. Ji, M. Oyamab, X. Liu and Y. He, *Electrochim. Acta*, 2013, **109**, 570-576.
30 F. Ren, H. Wang, C. Zhai, M. Zhu, R. Yue, Y. Du, P. Yang, J. Xu and W. Lu, *ACS Appl. Mater. Interfaces* 2014, **6**, 3607−3614.
31 J. Sun, X. Teng, J. Yang, H. Bi, *J. Mater. Sci.*, 2013, **48**, 8277–8286.
32 L. Li, Y. Wu, J. Lu, C. Nan and Y. Li, *Chem. Commun*, 2013, **49**, 7486-7488.
33 Y. Hu, H. Zhang, P. Wu, H. Zhang, B. Zhou and C. Cai, *Phys. Chem. Chem. Phy*, 2011, **13**, 4083-4094.
34 L. D. Zhu, T. S. Zhao, J. B. Xu and Z. X. Liang, *J. Power Sources*, 2009, **187**, 80-84.
35 A. Barinov, O. B. Malcioglu, S. Fabris, T. Sun, L. Gregoratti, M. Dalmiglio and M. Kiskinova, *J. Phys Chem. C*, 2009, **113**, 9009-9013.
36 J. Zhao, L. Zhan, H. Xue, Z. Wang and H. Hu, *RSC Adv*, 2012, **2**, 9651–9659.
37 S. J. Yoo, T. Y. Jeon, K. S. Kim, T. H. Lim and Y. E. Sung, *Phys. Chem. Chem. Phy,* 2010, **12**, 15240-15246.
38 A. V. Palenzuela, E. Brillas, C. Arias, F. Centellas, J. A. Garrido, R. M. Rodríguez and P. L. Cabot, *J. Power Sources*, 2013, **225**, 163-171.
39 C. Pan, L. Qiu, Y. Peng and F. Yan, *J. Mater. Chem*, 2012, **22**, 13578-13584.

Graphical Abstract

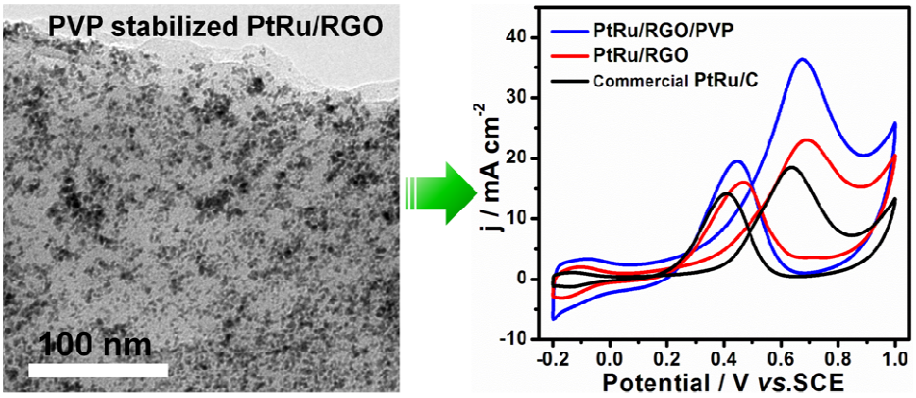

With assisted PVP surfactant, well-dispersion PtRu nanoclusters supported on the graphene surface and exhibited efficiently electrocatalytic activity and stability for the methanol oxidation.